

# PCCP

Accepted Manuscript



This is an *Accepted Manuscript*, which has been through the Royal Society of Chemistry peer review process and has been accepted for publication.

*Accepted Manuscripts* are published online shortly after acceptance, before technical editing, formatting and proof reading. Using this free service, authors can make their results available to the community, in citable form, before we publish the edited article. We will replace this *Accepted Manuscript* with the edited and formatted *Advance Article* as soon as it is available.

You can find more information about *Accepted Manuscripts* in the [Information for Authors](#).

Please note that technical editing may introduce minor changes to the text and/or graphics, which may alter content. The journal's standard [Terms & Conditions](#) and the [Ethical guidelines](#) still apply. In no event shall the Royal Society of Chemistry be held responsible for any errors or omissions in this *Accepted Manuscript* or any consequences arising from the use of any information it contains.

**Nature of the Interaction between Rare Gas Atoms and Transition  
Metal Doped Silicon Clusters: The Role of Shielding Effects**

**Vu Thi Ngan,<sup>a,\*</sup> Ewald Janssens,<sup>b</sup> Pieterjan Claes,<sup>b</sup>  
André Fielicke,<sup>c</sup> Minh Tho Nguyen,<sup>d</sup> and Peter Lievens<sup>b,\*</sup>**

*<sup>a)</sup> Department of Chemistry, Quy Nhon University, Quy Nhon, Vietnam*

*<sup>b)</sup> Laboratory of Solid State Physics and Magnetism, KU Leuven, B-3001 Leuven, Belgium*

*<sup>c)</sup> Institute for Optics and Atomic Physics, Technische Universität Berlin, Berlin, Germany*

*<sup>d)</sup> Department of Chemistry, KU Leuven, B-3001 Leuven, Belgium*

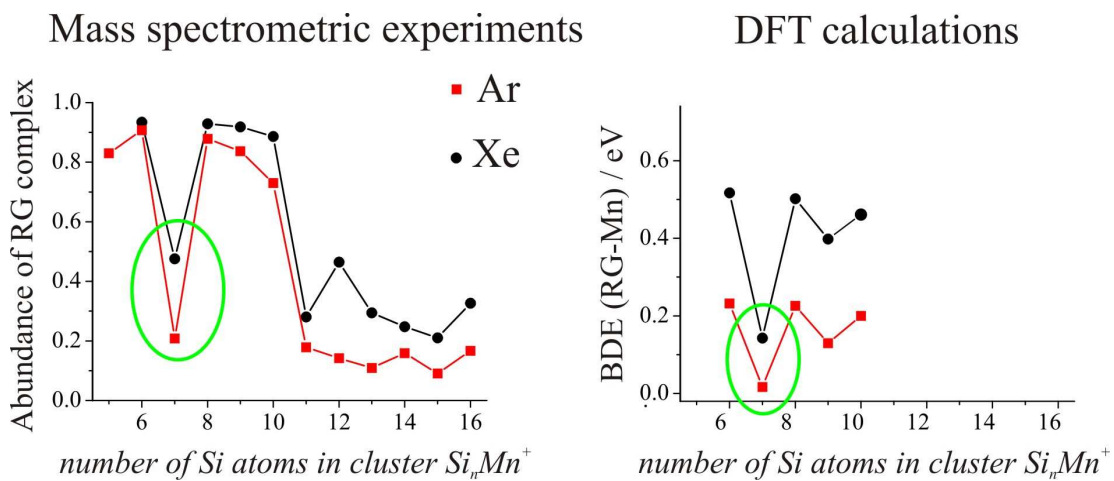
*Email: [vuthingan@qnu.edu.vn](mailto:vuthingan@qnu.edu.vn), [peter.lievens@fys.kuleuven.be](mailto:peter.lievens@fys.kuleuven.be)*

ABSTRACT: Mass spectrometry experiments show an exceptionally weak bonding between  $\text{Si}_7\text{Mn}^+$  and rare gas atoms as compared to other exohedrally transition metal (TM) doped silicon clusters and other  $\text{Si}_n\text{Mn}^+$  ( $n = 5-16$ ) sizes. The  $\text{Si}_7\text{Mn}^+$  cluster does not form Ar complexes and the observed fraction of Xe complexes is low. The interaction of two cluster series,  $\text{Si}_n\text{Mn}^+$  ( $n = 6-10$ ) and  $\text{Si}_7\text{TM}^+$  ( $\text{TM} = \text{Cr}, \text{Mn}, \text{Cu}$  and  $\text{Zn}$ ), with Ar and Xe is investigated by density functional theory calculations. The cluster-rare gas binding is for all clusters, except  $\text{Si}_7\text{Mn}^+$  and  $\text{Si}_7\text{Zn}^+$ , predominantly driven by short-range interaction between the *TM* dopant and the rare gas atoms. A high *s*-character electron density on the metal atoms in  $\text{Si}_7\text{Mn}^+$  and  $\text{Si}_7\text{Zn}^+$  shields polarization toward the rare gas atoms and thereby hinders formation of short-range complexes. Overall, both Ar and Xe complexes are similar except that the larger polarizability of Xe leads to larger binding energies.

**KEYWORDS:**

- cluster
- mass spectrometry
- messenger atom
- rare gas binding
- electron shielding effect

## TOC GRAPHIC



Density functional calculations and mass spectrometry reveal the role of a shielding effect from  $s$ -character electrons in the complexation between rare gas (Ar, Xe) and  $Si_nMn^+$  ( $n=6-10$ ),  $Si_7TM^+$  ( $TM=Cr, Mn, Cu$  and  $Zn$ ).

Atomic clusters emerge as interesting materials in the size regime between single atoms and nanoparticles, whose properties are strongly influenced by confinement effects. Understanding of their size and composition dependent structures and properties is primordial for further usage. The interactions between clusters and rare gas (RG) atoms are of crucial importance in many experimental techniques. For example, RG complexes are used for action spectroscopy in cluster science due to the inherent weak interaction,<sup>[1]</sup> Ar titration and tagging have been used to obtain isomer-specific photoelectron spectra for 2D and 3D gold clusters<sup>[2],[3]</sup> and isomer selective infrared (IR) spectra of niobium clusters.<sup>[4]</sup> In most experimental studies, it has been assumed that the RG atoms do not significantly influence the intrinsic structure and properties of the bare clusters, and are therefore called messenger or spectator atoms. A negligible influence of the RG atoms is inferred from their low adsorption energies and from insignificant differences in measured IR spectra of elemental clusters and their Ar-complexes, such as for  $V_n^+$ ,<sup>[5]</sup>  $Nb_n^+$ ,<sup>[6]</sup>  $Ta_n^+$  ( $n=6-20$ ),<sup>[7]</sup>  $Si_n^+$  ( $n=6-21$ ),<sup>[8]</sup> as well as for binary  $Si_nV^+$  and  $Si_nCu^+$  ( $n = 6-11$ ) clusters.<sup>[9]</sup> Nevertheless, such an assumption is not always applicable. Stronger cluster–RG interactions, which cause discernible changes in the IR spectra of the bare clusters, were observed for some  $Co_n^+$ ,  $Au_n$ , and doped  $Au_nY$  clusters.<sup>[10],[11],[12]</sup> Moreover, the RG tagging of some oxide clusters changes the energetic ordering of the isomers, in which case a low-energetic structural isomer, and thus not the ground state structure of the bare cluster, is probed in the experiment.<sup>[13]</sup> A simple electrostatic picture was put forward to explain the stronger influence of the RG atom, analogous to models often used to interpret the interaction of RG atoms with metal surfaces<sup>[14]</sup> or metal complexes.<sup>[15]</sup>

Much effort has been devoted to reveal the nature of interaction between RG and metal surfaces<sup>[12],[16]</sup> or metal-atom complexes.<sup>[14],[17]</sup> There are also a lot of experimental and theoretical results for transition metal cations interacting with RG atoms.<sup>[18]</sup> However,

only a few studies have been reported on RG interaction with clusters. In this letter, we demonstrate that the interaction of cationic transition metal (TM) doped silicon clusters with rare gas atoms is predominantly driven by short-range forces, while the long-range forces become dominant in some cases where the *s*-electron density on the TM atom along the principal axis hinders the formation of short-range RG complexes due to its shielding effect.

### Experimental Methods

Mass spectrometric experiments are performed in a molecular beam setup, which contains a dual target-dual laser vaporization cluster source<sup>[19]</sup> and a time-of-flight mass spectrometer. Two independent Nd:YAG lasers vaporize the target materials and create a plasma. Subsequent injection of a short pulse of helium cools the plasma and leads to condensation in the clustering channel. This condensation room is followed by a thermalization room, which is thermally isolated from the main body of the source and cooled by a continuous flow of liquid nitrogen. The source parameters are optimized for the formation of cold singly transition metal atom doped silicon clusters. A temperature controller allows for stabilization to any temperature in the 80–320 K range. The formation of cluster–argon and cluster–xenon complexes is induced by addition of a fraction of Ar or enriched <sup>129</sup>Xe to the He carrier gas, respectively. After expansion into vacuum the cluster distribution in the molecular beam is analyzed using a reflectron time-of-flight mass spectrometer.<sup>[20]</sup>

### Computational Methods

The clusters and their complexes are investigated computationally using density functional theory (DFT). The hybrid B3P86 functional is chosen because its good

performance for transition metal doped silicon clusters was proven in the previous studies in which computed vibrational spectra were compared with experimental infrared multiphoton dissociation (IR-MPD) spectra.<sup>[9,21]</sup> A comparison of other functionals including the M06 functional,<sup>[22]</sup> which is well known to be suitable for weakly bound system, has been already made in the previous study on the structure determination of  $\text{Si}_n\text{Mn}^+$ .<sup>[21]</sup> M06 calculations give similar energetics to B3P86, but still do not describe the system that well, even when including the RG ligands, at least in terms of the vibrational spectra. In the present study, the RG-cluster binding energies are also calculated using the two functionals (B3P86, M06) (cf. Table S1, Electronic Supplementary Information, ESI). In general, the M06 gives energetically the same picture as B3P86, but consistently  $\sim 0.1$  eV higher RG binding energies. Therefore, our discussion hereafter is only based on the B3P86 calculations.

The 6-311+G(d) basis set is applied for the silicon and transition metal atoms. The aug-cc-pVDZ-PP basis set, which explicitly treats up to 26 outer electrons, is used for the Xe atom and includes scalar relativistic effects that are important in predicting the binding energies between metal ions and rare gas atoms.<sup>[23]</sup> All calculations are performed using the Gaussian 03 package.<sup>[24]</sup> Natural population analysis is done using the NBO 5.G program. All energies are corrected with zero-point energies (ZPEs) computed at the same level of theory.

### ***Mass spectrometric observations***

Typical mass spectra of rare gas complexes of manganese doped cationic silicon,  $\text{Si}_n\text{Mn}_m^+\cdot\text{RG}$  ( $n = 7-17$ ,  $m = 0-2$ ,  $\text{RG} = \text{Ar}$  and  $\text{Xe}$ ), are shown in Figure 1. The upper trace shows manganese doped silicon clusters and their argon complexes measured with the cluster source at 80 K and 1% of Ar in the He carrier gas. The mass spectrum in the

lower trace is measured using 0.5% of isotopically enriched xenon ( $^{129}\text{Xe}$ ) in the carrier gas and the source at 120 K. The xenon atom is able to attach even to the silicon at this temperature and therefore, additionally to  $\text{Si}_n\text{Mn}_m^+\cdot\text{Xe}$ , Xe-complexes are seen for the pure silicon clusters.

The relative intensities of the different species were obtained by fitting the natural isotope distributions of the different species to the measured mass spectra. This way partly overlapping species (because of the isotopic broadening) have been deconvoluted. This is required since the atomic mass of Mn is only 1 u less than twice that of the most abundant  $^{28}\text{Si}$  isotope and thus significant overlap of the isotopic patterns of pure  $\text{Si}_{n+2}^+$ ,  $\text{Si}_n\text{Mn}^+$ , and  $\text{Si}_{n-2}\text{Mn}_2^+$  takes place. As an example the resulting intensities obtained in the measurements using Ar are plotted in Figure S1 in the ESI for  $\text{Si}_n^+$ ,  $\text{Si}_n\text{Mn}^+$ ,  $\text{Si}_n\text{Mn}_2^+$ ,  $\text{Si}_n\text{Mn}^+\cdot\text{Ar}$ ,  $\text{Si}_n\text{Mn}^+\cdot\text{Ar}_2$ , and  $\text{Si}_n\text{Mn}_2^+\cdot\text{Ar}$ . From this, the cluster size dependent fraction of RG complexes can then be calculated. This fraction is defined as

$$F_{\text{RG}} = \frac{I(\text{Si}_n\text{Mn}^+\cdot\text{RG}) + I(\text{Si}_n\text{Mn}^+\cdot\text{RG}_2)}{I(\text{Si}_n\text{Mn}^+) + I(\text{Si}_n\text{Mn}^+\cdot\text{RG}) + I(\text{Si}_n\text{Mn}^+\cdot\text{RG}_2)}$$

with  $I(\text{Si}_n\text{Mn}^+)$ ,  $I(\text{Si}_n\text{Mn}^+\cdot\text{RG})$ , and  $I(\text{Si}_n\text{Mn}^+\cdot\text{RG}_2)$  representing the integrated abundances of the cluster, its RG and  $\text{RG}_2$  complexes, respectively. These fractions are plotted in Figure 2a for  $\text{Si}_n\text{Mn}^+\cdot\text{RG}$  ( $n = 5-16$ ) for  $\text{RG} = \text{Ar}$  (red squares) and  $\text{RG} = \text{Xe}$  (black dots).



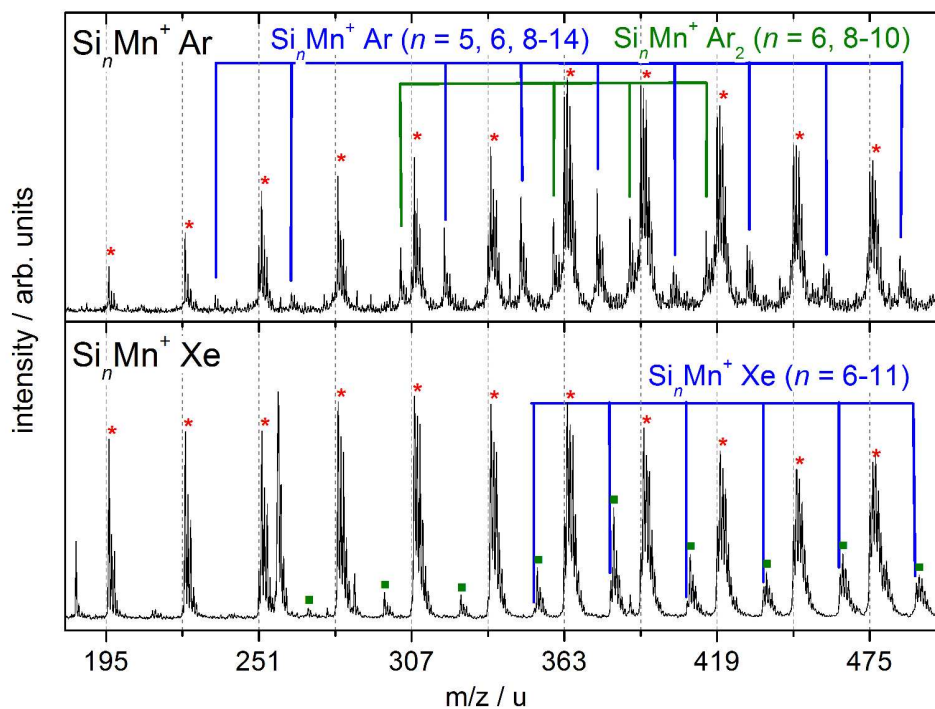


**Figure 1.** Mass spectra showing the formation of complexes of  $\text{Si}_n\text{Mn}^+$  with Ar (upper trace) and Xe (lower trace). Bare silicon and  $\text{Si}_n^+-\text{Xe}$  clusters are marked with red stars and green squares, respectively. Manganese doped silicon clusters are represented by the grid lines, doped cluster- $RG$  ( $RG = \text{Ar}, \text{Xe}$ ) complexes are indicated by blue lines and cluster- $\text{Ar}_2$  complexes by green lines. The detailed experimental conditions are given in the text.

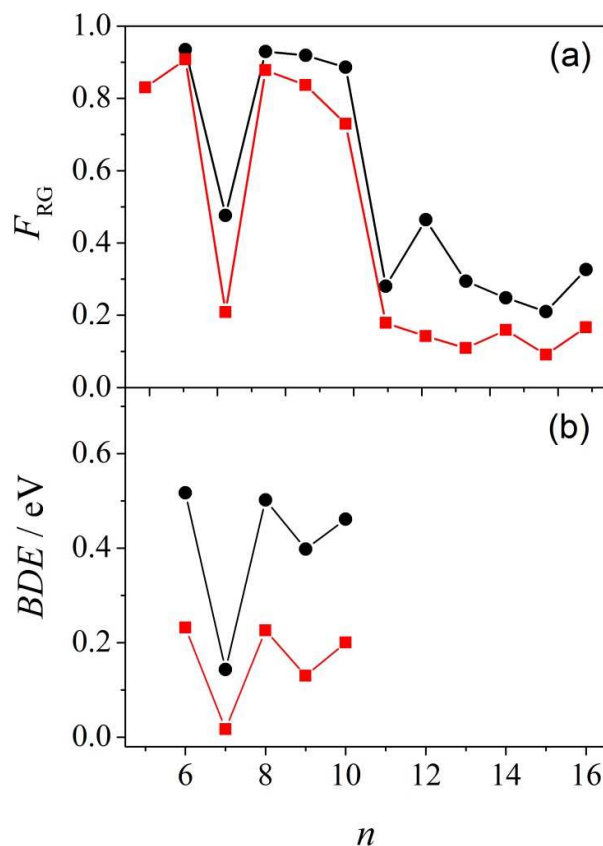


**Figure 2.** (a) Cluster size dependent fraction of  $RG$  complexes,  $F_{RG}$ , for  $Si_nMn^+$  ( $n=5-16$ ) for  $RG = Ar$  (red squares) and  $RG = Xe$  (black dots). (b) Calculated cluster size dependent binding energies between the  $Si_nMn^+$  ( $n=6-10$ ) and  $Ar$  (red squares) and  $Xe$  (black dots), respectively.

The degree of  $RG$  complex formation can provide precious structural information.<sup>2,3,24</sup> It was, for example, previously demonstrated that no  $Ar$ -complex formation was possible (at 80 K) on pure cationic silicon clusters or on endohedral TM-doped silicon cations, while  $Ar$  does adsorb on cationic exohedrally TM-doped (Ti, V, Cr, Co, or Cu) Si clusters.<sup>[25]</sup> Because of its higher polarizability,  $Xe$  complexes have been observed for both pure Si clusters and endohedral TM-doped Si clusters.<sup>[8],[26]</sup>

The propensity for  $RG$  complex formation, as observed in Fig. 2a, is expected to depend on the strength of the bond between the  $Si_nMn^+$  cluster and the  $RG$  atom. The reduced complex formation at the critical size of  $n = 11$  is attributed to the encapsulation

of the dopant atom from this size onwards, in line with the observations for other dopants (Ti, V, Cr, Co, and Cu).<sup>[25]</sup> Surprisingly, the propensity of Ar and Xe complex formation for  $\text{Si}_7\text{Mn}^+$  is exceptionally low, an effect that has not been observed for any of the other TM dopants studied before. In order to explain why the fraction of  $\text{Si}_7\text{Mn}^+\cdot\text{RG}$  complexes is so much lower than those of other  $\text{Si}_n\text{Mn}^+$  ( $n \leq 10$ ) clusters, we set out a theoretical study of the chemical bonding of Ar and Xe atoms with two series of clusters:  $\text{Si}_n\text{Mn}^+$  ( $n = 6-10$ ) and  $\text{Si}_7\text{TM}^+$  ( $\text{TM} = \text{Cr, Mn, Cu, and Zn}$ ). The former series allows the size-dependence of the interaction to be studied, while the latter series concentrates on the role of the electron configuration of the dopant atom.

#### *Interaction between $\text{Si}_n\text{Mn}^+$ ( $n = 6-10$ ) and Ar, Xe atoms*

Structures of  $\text{Si}_n\text{Mn}^+$  clusters were unambiguously identified on the basis of a comparison between measured infrared multiple photon dissociation spectra on the cluster-rare gas complexes and calculated harmonic vibrational counterparts using DFT at the B3P86/6-311+G(d) level.<sup>[21]</sup> The potential energy surface of the cluster was carefully investigated by searching various structural isomers at different possible spin states. The  $\text{Si}_n\text{Mn}^+$  clusters were concluded to favor the high-spin states such as septet and quintet, while low-spin states (singlet and triplet states) are less stable. These results were later on confirmed by the X-ray magnetic circular dichroism (XMCD) spectroscopy.<sup>[27]</sup>

In the present study we focus on the cluster-rare gas interaction in the experimentally observed complexes. Structurally, only the exact binding position of the rare gas atom is unsure, as the available IR spectrum was not very sensitive to this. We therefore have searched different isomers of the rare gas complexes and found only two isomers for  $\text{Si}_7\text{Mn}^+\cdot\text{RG}$  and one stable isomer for other  $\text{Si}_n\text{Mn}^+\cdot\text{RG}$ . Due to the weak interaction, the rare gas attachment does not lead to changes in the electronic/spin state of the clusters.

The most stable structure of the complexes, consisting of cationic  $\text{Si}_n\text{Mn}^+$  ( $n = 6-10$ ) and  $RG = \text{Ar}$  or  $\text{Xe}$ , are presented in Figure 3. For  $\text{Si}_7\text{Mn}^+\cdot RG$ , two stable structural isomers, **Com-A** and **Com-B**, have been identified. The  $RG$  directly binds to the Mn dopant atom along an axis connecting the Mn atom with the center of the cluster (principal axis). **Com-B** of  $\text{Si}_7\text{Mn}^+\cdot RG$  is an exception in which the  $RG$  is bound to the Mn dopant in such a way that the Mn- $RG$  bond is nearly perpendicular to the  $C_2$  axis of  $\text{Si}_7\text{Mn}^+$  cation.

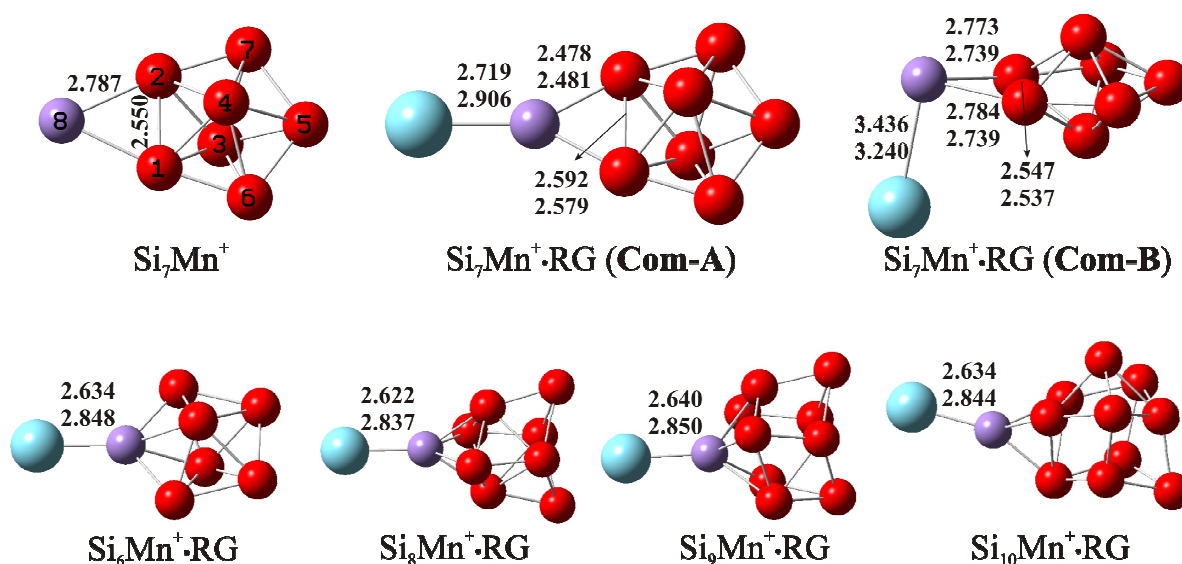


**Figure 3.** Structures of  $\text{Si}_n\text{Mn}^+\cdot RG$  ( $n = 6-10$ ,  $RG = \text{Ar}$ ,  $\text{Xe}$ ). Red spheres are Si atoms, purple spheres Mn atoms and blue spheres  $RG$  atoms. Selected bond lengths are given in Å, the upper values are for the Ar-complexes, and the lower values are for the Xe-complexes. The numbering of the atoms of  $\text{Si}_7\text{Mn}^+$  is applied also for its  $RG$  complexes.

The  $\text{Si}_n\text{Mn}^+-RG$  bond dissociation energy ( $BDE$ ) is calculated as:

$$BDE(\text{Si}_n\text{Mn}^+\cdot RG) = E(\text{Si}_n\text{Mn}^+) + E(RG) - E(\text{Si}_n\text{Mn}^+\cdot RG)$$

$BDE$  amounts to  $\sim 0.1-0.2$  eV for  $\text{Si}_n\text{Mn}^+\cdot \text{Ar}$  and  $\sim 0.4-0.5$  eV for  $\text{Si}_n\text{Mn}^+\cdot \text{Xe}$  with  $n = 6, 8-10$ . For  $\text{Si}_7\text{Mn}^+$  much smaller  $BDE$  are found. The stationary structure **Com-A** of  $\text{Si}_7\text{Mn}^+\cdot \text{Ar}$  even has negative  $BDE$  after correction for ZPEs, meaning that such a complex will only be metastable. **Com-A** of  $\text{Si}_7\text{Mn}^+\cdot \text{Xe}$  has an exceptionally low  $BDE$  of

only 0.03 eV. The *BDE* of **Com-B** is 0.02 eV for  $\text{Si}_7\text{Mn}^+\cdot\text{Ar}$  and 0.14 eV for  $\text{Si}_7\text{Mn}^+\cdot\text{Xe}$ . Complexes with a *BDE* larger than  $\sim 0.15$  eV (such as for  $\text{Si}_n\text{Mn}^+\cdot\text{RG}$  with  $n = 6, 8-10$  and  $\text{RG} = \text{Ar}, \text{Xe}$ ) are observed in the mass spectra with higher abundances. Calculations using the M06 functional that also accounts for dispersion interactions give a similar picture, but the interaction energies are consistently  $\sim 0.1$  eV higher (Table S1, ESI). These *BDE* values are consistent with the typical adsorption energies of *RG* on metal surfaces (being  $\sim 0.1-0.2$  eV).<sup>[28]</sup> The lower *BDE* of **Com-B**, for both  $\text{RG} = \text{Ar}$  and  $\text{RG} = \text{Xe}$ , is in line with the low fraction of *RG* complexes observed for  $\text{Si}_7\text{Mn}^+$  (cf. Figure 2a). For the ease of comparison, the dependence of the computed *BDE* on the cluster size is plotted in Figure 2b. Qualitatively, this plot reproduces the size dependence of the *RG* complex formation on cluster size in Figure 2a. In summary, using DFT calculations, we could reproduce the peculiar behavior of the  $\text{Si}_7\text{Mn}^+$  toward *RG* atoms and conclude that the calculated *BDE* is proportional to  $F_{\text{RG}}$ .

In an attempt to explain the exceptionally low  $BDE(\text{RG}-\text{Si}_7\text{Mn}^+)$  of **Com-A** and **Com-B**, the nature of interaction between  $\text{Si}_n\text{Mn}^+$  and *RG* atoms is analyzed. For  $n = 6, 8-10$ , the Mn-*RG* distance is calculated to be around 2.6 and 2.8 Å for Ar and Xe, respectively. **Com-A** of  $\text{Si}_7\text{Mn}^+$  has slightly larger bond lengths of 2.7 and 2.9 Å for Ar and Xe, respectively. Assuming that the nature of interaction in **Com-A** is similar to that of the  $\text{Si}_n\text{Mn}^+\cdot\text{RG}$  ( $n = 6, 8-10$ ) complexes, the difference in bond length indicates that the *RG* interaction with  $\text{Si}_7\text{Mn}^+$  in **Com-A** is expected to be weaker than that with other cluster sizes. Although **Com-B** of  $\text{Si}_7\text{Mn}^+$  is energetically more stable than **Com-A**, the Mn-*RG* distances in **Com-B** are much longer, being 3.44 and 3.24 Å for Ar and Xe, respectively. Noting that both complexes have a septet electronic state as also the bare  $\text{Si}_7\text{Mn}^+$  cluster, the nature of the cluster-*RG* interactions in the **Com-A** and **Com-B** must differ significantly from each other.

Four factors usually contribute to the binding energy of complexes: (i) overlap of orbitals from the two interacting fragments (i.e., cluster and RG atom) leading to a polarization and charge transfer; (ii) repulsion between occupied orbitals of the two fragments; (iii) polarization contribution of the RG atom caused by a positive charge at the binding site (i.e., the Mn dopant atom), and (iv) long-range interaction forces caused by higher-order polarization effects and dispersion energy. The last factor is dominant in the case of no orbital overlap. Of these four factors, (ii) induces a decrease in binding energy while the other three tend to increase the bond strength.

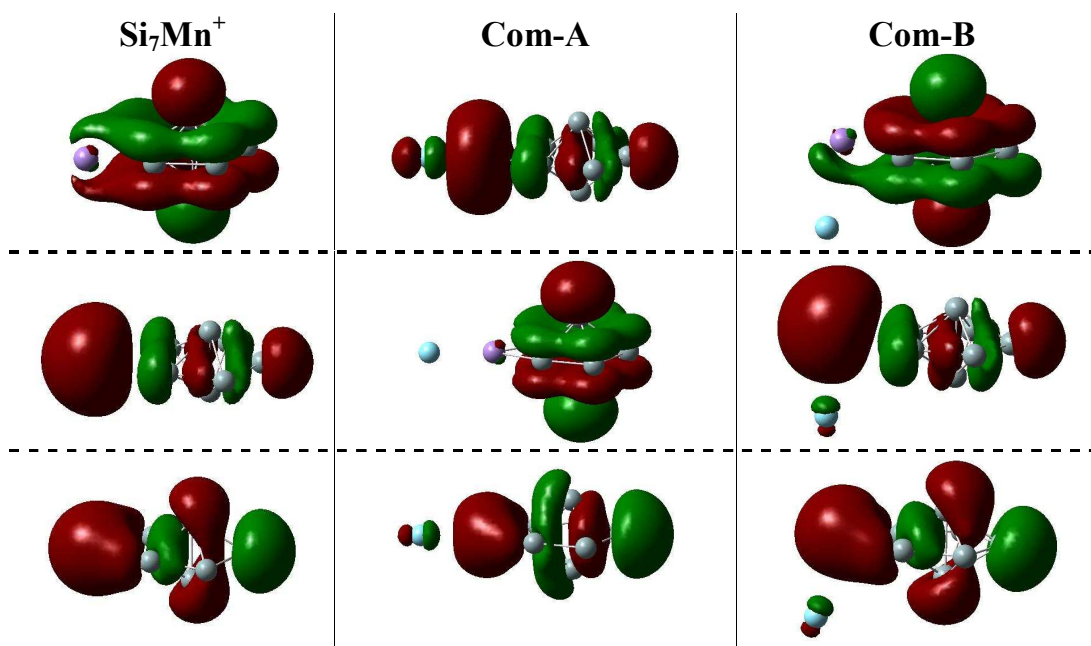


**Figure 4.** Selected frontier orbitals of  $\text{Si}_7\text{Mn}^+$  and **Com-A**, **Com-B** of  $\text{Si}_7\text{Mn}^+\cdot\text{Ar}$ . The upper row shows the LUMOs, the middle row the HOMOs, the lower row the HOMO-5 for the bare cluster and **Com-B**, and the HOMO-3 for **Com-A**. Purple spheres are Mn atoms, grey spheres Si atoms and blue spheres Ar atoms.

Let us now analyze in detail these different contributions to the *BDE* of the  $\text{Si}_n\text{Mn}^+\cdot\text{RG}$  ( $n = 6-10$ ,  $\text{RG} = \text{Ar}, \text{Xe}$ , **Com-A** considered for  $\text{Si}_7\text{Mn}^+$ ) complexes.

i) A careful investigation of the valence molecular orbitals (MOs) of the  $\text{Si}_n\text{Mn}^+$  clusters and their RG-complexes points out that the  $np$  atomic orbitals (AOs) of the RG atom ( $3p$  for Ar and  $5p$  for Xe) strongly overlap with MOs having large contributions of  $3d$  AO(Mn) of  $\text{Si}_n\text{Mn}^+$ , causing a charge transfer of  $\sim 0.1$  e from Ar to Mn, and  $\sim 0.2$  e from Xe to Mn. However, the orbital overlaps in the complexes of  $\text{Si}_7\text{Mn}^+$  are weaker, thereby leading to a smaller charge transfer (being only 0.07 and 0.14 e for the Ar- and Xe-complex, respectively). In combination with the earlier discussed size dependence of the  $\text{Si}_n\text{Mn}^+ \text{--} \text{RG}$  bond length, it can be concluded that the orbital overlap contribution to the *BDE* of the  $\text{Si}_n\text{Mn}^+ \cdot \text{RG}$  ( $n = 6, 8\text{--}10$ ) complexes is significant, while it is smaller for  $\text{Si}_7\text{Mn}^+ \cdot \text{RG}$ . The *RG* atom is thus less polarized by interaction with MOs of  $\text{Si}_7\text{Mn}^+$  than by MOs of the other  $\text{Si}_n\text{Mn}^+$  sizes. Natural population analysis of the occupation of Mn orbitals in  $\text{Si}_n\text{Mn}^+$  provides us with two reasons for the special behavior of  $\text{Si}_7\text{Mn}^+$ . Firstly, both the  $3d$  and  $4s$  shells of Mn in  $\text{Si}_7\text{Mn}^+$  are half-filled ( $3d^5 4s^1$ ) while in the other cluster sizes there are nearly 6 electrons in the Mn  $3d$  orbitals ( $3d^6 4s^0$ ). The half-filled Mn  $3d$  shell in  $\text{Si}_7\text{Mn}^+$  is more stable than the Mn  $3d^6$  configuration of the other  $\text{Si}_n\text{Mn}^+$  sizes, leading to a smaller polarization toward AO- $np$  (*RG*). Secondly, the large electron density of AO- $4s$  (Mn) of  $\text{Si}_7\text{Mn}^+$  hinders polarization of  $3d$  orbitals (Mn) toward AO of *RG*. This can be considered as a shielding or screening effect. Similar shielding effects likely also hamper the formation of a bond between the isolated  $\text{Mn}^+$  cation ( $3d^5 4s^1$ ) and Ar.<sup>[18]</sup> It should be noted, however, while the IR-MPD spectrum for  $\text{Si}_7\text{Mn}^+ \cdot \text{Xe}$  gives favorable agreement for the calculated spectrum of the isomer shown in Figure 3 with the  $3d^5 4s^1$  local configuration at the Mn atom,<sup>21</sup> an independent experimental study finds a magnetic moment at the Mn of only  $4 \mu_B$ .<sup>[27]</sup>

ii) It is found that the repulsion contribution is negligible in  $\text{Si}_n\text{Mn}^+ \cdot \text{RG}$  complexes for  $n = 6, 8\text{--}10$ , whereas it is significant for  $\text{Si}_7\text{Mn}^+ \cdot \text{RG}$ . Indeed,  $\text{Si}_7\text{Mn}^+$  has two occupied

MOs (HOMO and HOMO-5, Figure 4) having large contributions of AO-4s (Mn). These MOs are characterized by large lobes along the  $C_2$  axis and pointing out the  $\text{Si}_7\text{Mn}^+$  molecule, which is elucidated by its Mn  $3d^54s^1$  electronic configuration. The contribution of AO-4s (Mn) to the MO of  $\text{Si}_7\text{Mn}^+$  is pictorially emphasized by plots of total and partial density of states shown in Figure S2 of the ESI. The HOMO and HOMO-5 of  $\text{Si}_7\text{Mn}^+$  cause a strong repulsion upon interaction with the occupied AO- $np$  of the  $RG$  atom along the  $C_2$  axis. As a result, their energies largely increase in **Com-A** of  $\text{Si}_7\text{Mn}^+\cdot\text{Ar}$  leading to a change in the energetic ordering of the MOs relative to those of bare  $\text{Si}_7\text{Mn}^+$  (cf. Figure 4). In particular, the HOMO of  $\text{Si}_7\text{Mn}^+$  correlates with the complex's LUMO, and the LUMO of the  $\text{Si}_7\text{Mn}^+$  with the complex's HOMO. The swap between HOMO and LUMO destabilizes **Com-A**, which is witnessed by its negative  $BDE$ . A similar reasoning holds for **Com-A** of  $\text{Si}_7\text{Mn}^+\cdot\text{Xe}$ . But the larger polarizability of Xe, which compensates the negative contribution of the repulsion, results in a small positive  $BDE$  of 0.03 eV.

iii) The dipolar polarization significantly contributes to the binding energy as the positive charges on the Mn atoms in  $\text{Si}_n\text{Mn}^+$  are rather large, amounting to  $\sim 0.8$ -1.0 e. However, for  $\text{Si}_7\text{Mn}^+$ , the existence of a big lobe of  $s$ -character electron density on the  $C_2$  axis prevents the polarization of the charge of Mn toward the  $RG$  atoms, due to the shielding effect. In this case, the shielding of the AO-4s(Mn) has a two-fold effect including the less effective nuclear charge (leading to the weaker polarizability by charge) and the less orbital overlap between AO-3d(Mn) and AO-3p(Ar)/5p(Xe).

iv) The long-range contribution which is caused by higher-order polarization and dispersion is expected to be much smaller than the other three contributions because of the relatively short bond lengths in these complexes.



In summary, the binding energy of the  $\text{Si}_n\text{Mn}^+\cdot\text{RG}$  ( $n = 6, 8-10$  and  $\text{RG} = \text{Ar, Xe}$ ) complexes is mainly determined by the polarization of the  $\text{RG}$  atoms by the orbital overlap and the large positive charge on Mn. Such bonding mechanism is similar to the familiar explanation for the short-range  $\text{RG}$  interaction with metal surfaces and metal complexes.<sup>[29]</sup> The interaction in **Com-A** of  $\text{Si}_7\text{Mn}^+$  is different. There are two positive and one negative contribution to its  $BDE$ . The positive contributions include the polarizations by orbital overlap and by positive charge on Mn, but they are smaller than those of the other cluster sizes due to the screening effect of the  $\text{AO-4s}$  on the Mn dopant.

We now turn to an understanding of the nature of chemical bonding in **Com-B** of  $\text{Si}_7\text{Mn}^+\cdot\text{Ar}$  and  $\text{Si}_7\text{Mn}^+\cdot\text{Xe}$ . The different contributions to the  $BDE$  of **Com-B** in comparison with **Com-A** are as follows:

i) Comparing the MOs of **Com-A** and **Com-B** of  $\text{Si}_7\text{Mn}^+$  we find that the orbital overlap contribution is much smaller in **Com-B** than that in **Com-A**. Indeed, the charge transfer from  $\text{RG}$  to Mn in **Com-B** is only 0.01 and 0.07 electron for Ar and Xe, respectively, as compared to values of 0.07 and 0.14 electron for **Com-A** with Ar and Xe.

ii) The repulsion contribution in **Com-B** is much weaker than that in **Com-A**, because the  $4s$  electron density located out of the  $C_2$  axis is smaller than those on the axis. Therefore the ordering of MOs in **Com-B** is similar to that in the  $\text{Si}_7\text{Mn}^+$  cluster and there is no switch between HOMO and LUMO of  $\text{Si}_7\text{Mn}^+$  upon formation of **Com-B** (cf. Figure 4).

iii) Due to the weaker effect of out-of-axis  $s$ -electrons, the polarization contribution of the positive charge of Mn towards the  $\text{RG}$  atom is larger in **Com-B** than in **Com-A**.

iv) The long-range contribution plays a more important role to  $BDE(\text{Com-B})$  due to the absence of orbital overlap, which leads to a long distance between Mn and  $\text{RG}$

atoms. Moreover, the *RG* atom in **Com-B** is not only interacting with the Mn but also with the Si atoms (numbered 1, 2 and 3 in Figure 3).

In summary, for **Com-B** of  $\text{Si}_7\text{Mn}^+$  the polarization by orbital overlap and repulsion contributes much less to the bonding, whereas the polarization by positive charge and long-range effects including dipole and higher-order polarization bring about the most important parts to the *BDE*. Due to the main contribution of polarization, the Xe atom possessing higher polarizability interacts stronger with  $\text{Si}_7\text{Mn}^+$  than the Ar atom, leading to the remarkable observation that the Mn–Xe bond distance (3.24 Å) is shorter than the Mn–Ar distance (3.44 Å) in **Com-B**.

Hence, the nature of the interactions between the *RG* atoms and  $\text{Si}_n\text{Mn}^+$  ( $n = 6, 8-10$ ) is predominantly characterized by a polarization of the *RG* atom due to the orbital overlap and to the positive charge on the Mn dopant. This model for the interaction was used to rationalize the bonding of *RG* with several pure or doped Si clusters<sup>[25]</sup> and in the  $\text{Co}_n^+\cdot\text{Ar}$  ( $n = 4-8$ ) metal cluster complexes.<sup>[10]</sup> It is also a popular model to explain the interaction of *RG* atoms with metal surfaces and metal ion complexes.<sup>[14, 17, 29]</sup> Avoidance of the symmetrical axis for binding was also found for the  $\text{Mn}^+\cdot(\text{H}_2\text{O})$  complex.<sup>[15]</sup>

### ***Interaction between $\text{Si}_7\text{TM}^+$ with $\text{TM} = \text{Cr}, \text{Mn}, \text{Cu}, \text{Zn}$ and $\text{Ar}, \text{Xe}$***

The role of the electronic structure of the dopant atom is unraveled by studying the cluster–*RG* interaction along the  $\text{Si}_7\text{TM}^+$  series with  $\text{TM} = \text{Cr}, \text{Mn}, \text{Cu},$  and  $\text{Zn}$ . The clusters are assumed to all have a *TM*-capped pentagonal bipyramidal structure with  $\text{C}_{2v}$  symmetry. The  $\text{Si}_7\text{Cr}^+$ ,  $\text{Si}_7\text{Mn}^+$ , and  $\text{Si}_7\text{Cu}^+$  structures have been identified by combined IRMPD spectroscopy and DFT studies.<sup>[9,21,30]</sup> No IRMPD data are available to confirm the computed structure for  $\text{Si}_7\text{Zn}^+$ . The clusters have  ${}^6\text{A}_1$ ,  ${}^7\text{A}_1$ ,  ${}^1\text{A}_1$ , and  ${}^2\text{A}_1$  ground electronic states for  $\text{Si}_7\text{Cr}^+$ ,  $\text{Si}_7\text{Mn}^+$ ,  $\text{Si}_7\text{Cu}^+$ , and  $\text{Si}_7\text{Zn}^+$ , respectively. For each cluster

isomer we have investigated different spin states from singlet up to octet and there is a little doubt about the ground electronic state of the investigated clusters. The  $\text{Si}_7\text{Cr}^+$ ,  $\text{Si}_7\text{Mn}^+$  favor high-spin states while  $\text{Si}_7\text{Cu}^+$ , and  $\text{Si}_7\text{Zn}^+$  favor low-spin states, alike the corresponding isolated metal cations. The isolated cations  $\text{Cr}^+$  ( $[\text{Ar}]3d^54s^0$ ) and  $\text{Mn}^+$  ( $[\text{Ar}]3d^54s^1$ ) have half-filled  $3d$  shells, while the  $\text{Cu}^+$  ( $[\text{Ar}]3d^{10}4s^0$ ) and  $\text{Zn}^+$  ( $[\text{Ar}]3d^{10}4s^1$ ) have totally filled  $3d$  shells. Comparison of the RG interaction with  $\text{Si}_7\text{Zn}^+$  and  $\text{Si}_7\text{Cu}^+$  to that with  $\text{Si}_7\text{Mn}^+$  reveals a stabilizing role of the filled versus and half-filled  $3d$  shell in the RG interaction of the TM-capped pentagonal bipyramidal silicon clusters. Comparing the interaction of RG atoms with  $\text{Si}_7\text{Cr}^+$  to that with  $\text{Si}_7\text{Mn}^+$  emphasizes the role of the shielding effect of the  $s$ -electron in the bonding.

Complex **Com-A** with an Ar atom is only metastable for  $\text{Si}_7\text{Mn}^+$  while it is stable for  $\text{Si}_7\text{Cu}^+$  and  $\text{Si}_7\text{Cr}^+$  with the *BDEs* of 0.22 and 0.19 eV, respectively, even though the Ar–*TM* bond lengths in  $\text{Si}_7\text{Cu}^+\cdot\text{Ar}$  and  $\text{Si}_7\text{Cr}^+\cdot\text{Ar}$  (2.46 and 2.82 Å, respectively) are comparable to that in **Com-A** of  $\text{Si}_7\text{Mn}^+\cdot\text{Ar}$ . This result means that the nature of interaction of the Ar atoms with  $\text{Si}_7\text{Cu}^+$  and  $\text{Si}_7\text{Cr}^+$  is different from that of Ar with  $\text{Si}_7\text{Mn}^+$ . A similar conclusion can be drawn for the corresponding Xe-complexes (cf. ESI).

Similar to  $\text{Si}_7\text{Mn}^+$ ,  $\text{Si}_7\text{Zn}^+$  forms two complexes **Com-A** and **Com-B** with *BDE* values of -0.40 and 0.01 eV for Ar, and -0.11 and 0.10 eV for Xe, respectively. This indicates that the nature of the RG interaction with  $\text{Si}_7\text{Zn}^+$  and  $\text{Si}_7\text{Mn}^+$  is rather similar. However the *BDEs* of the *RG* complexes of  $\text{Si}_7\text{Zn}^+$  are even lower than those of  $\text{Si}_7\text{Mn}^+$ . Experimentally, no adsorption of Ar on  $\text{Si}_n\text{Zn}^+$  clusters is observed.

To investigate further the orbital overlap, the overlap populations (based on the C-squared population analysis, SCPA<sup>[31]</sup>) between the AOs of Ar and *TM* dopant atoms in **Com-A** of  $\text{Si}_7\text{TM}^+\cdot\text{Ar}$  are plotted in Figure 5. It can be seen that the orbital overlaps for *TM* = Cr, Cu are much stronger than for *TM* = Mn, Zn. The AO- $3s(\text{Ar})$  hardly participate

in the overlap, and therefore are not shown in Figure 5. The AO-3p(Ar) overlap strongly with the AO-3d, 4s, and 4p of  $TM = Cr$  or  $Cu$ . The AO-3d( $TM$ ) overlap less with AO-3p(Ar) in  $Si_7Mn^+ \cdot Ar$  and the population overlap becomes even zero in the case of  $Si_7Zn^+ \cdot Ar$ . For the latter, there only is overlap between AO-4p (Zn) and AO-3p (Ar), meaning that the shielding effect of Zn is so strong that the AOs-3d do not participate at all in the overlap, which leads to a polarization.

The valence electronic configuration of the  $TM$  atom in the bare cluster  $Si_7TM^+$  computed using NBO analysis are  $[3d^{4.9} 4s^{0.2}]$ ,  $[3d^{5.1} 4s^{1.0}]$ ,  $[3d^{9.9} 4s^{0.3}]$  and  $[3d^{10.0} 4s^{1.2}]$  for  $TM = Cr, Mn, Cu,$  and  $Zn$ , respectively. Both Cr and Mn thus maintain their half-filled  $3d^5$  shell, while both Cu and Zn atoms have a filled  $3d^{10}$  shell in the  $Si_7TM^+$  clusters. The electron populations of the Mn and Zn 4s orbitals in the  $Si_7TM^+$  clusters are much larger than those of Cr and Cu. Therefore, the weak orbital overlap of  $Si_7Mn^+$  and  $Si_7Zn^+$  is not related to the stability of half-filled or filled 3d shells of the TM atom, but rather to shielding effects of their 4s electrons.

Regarding the shapes of the frontier MOs (Table S6 of the ESI), the  $Si_7TM^+$  ( $TM = Cr, Mn, Cu,$  and  $Zn$ ) clusters have similar LUMOs. The  $Si_7Mn^+$  and  $Si_7Zn^+$  clusters have a similar HOMO with a large  $s$ -lobe along the  $C_2$  axis whereas  $Si_7Cr^+$  and  $Si_7Cu^+$  have a HOMO with a nodal plane containing the  $C_2$  axis. The MOs with a large  $s$ -character on the  $C_2$  axis are unoccupied in the latter. Swaps of HOMO and LUMO, relative to the bare clusters, are found for  $Si_7Mn^+$  and  $Si_7Zn^+$  when forming **Com-A** but not for **Com-B**.

In all cases, the Xe-complexes are similar to the Ar-complexes, except that the polarizability of Xe is larger than that of Ar, leading to larger polarization energies and thus larger  $BDEs$  of the Xe-complexes.

### Conclusions

In conclusion, the nature of the interactions of *RG* atoms with most of the investigated exohedral transition metal doped silicon cluster cations ( $\text{Si}_n\text{Mn}^+$  with  $n = 6, 8-10$  and  $\text{Si}_7\text{TM}^+$  with  $\text{TM} = \text{Cr}, \text{Cu}$ ) are predominantly characterized by a polarization of the *RG* atom due to the orbital overlap and the positive charge of the clusters. Both Ar and Xe atoms can form similar complexes, but the interaction of the dopant atoms with Xe is stronger due to a larger polarizability related to the larger size of the Xe atom.  $\text{Si}_7\text{Mn}^+$  and  $\text{Si}_7\text{Zn}^+$  appear to be special cases. The *RG* atom tends to avoid binding with the Mn and Zn dopants on the  $C_2$  axis to form **Com-A** due to a shielding effect of the dopant *s*-electron density. Formation of  $\text{Si}_7\text{TM}^+\cdot\text{RG}$  complexes having the **Com-B** shape is essentially characterized by long-range interaction forces.

The findings of the present study can be generalized as follows: clusters having high electron density of *s*-character toward the principal axis of the molecule are expected to be prevented from complexing by a polarization of the *RG* atom and a repulsion with the occupied orbitals of the *RG* atoms, overall leading to a weaker interaction energy in the resulting *RG*-complexes, and thereby limiting the formation of the latter.

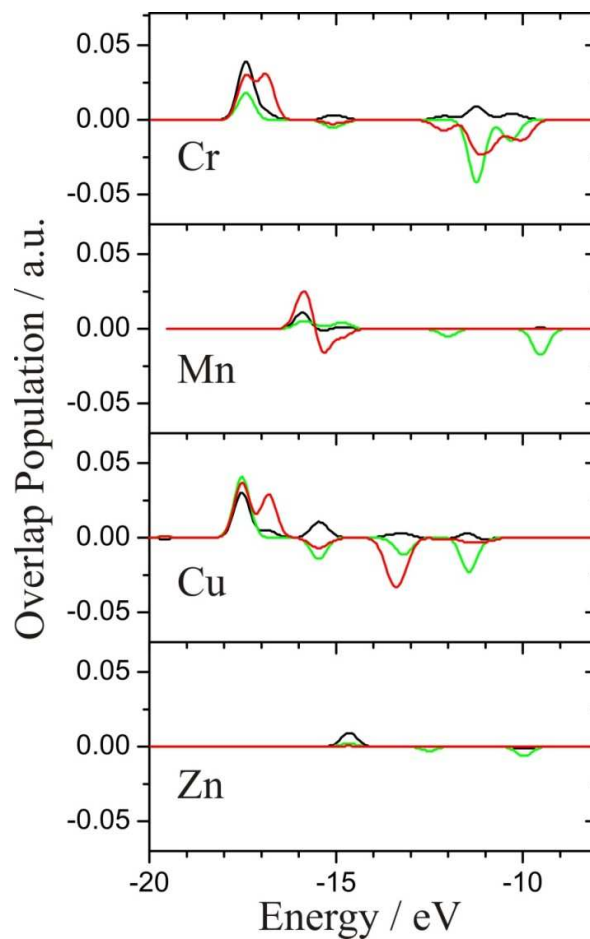


**Figure 5.** Overlap population between atomic orbitals of Ar and the *TM* dopant atoms in **Com-A** of  $\text{Si}_7\text{TM}^+$  ( $\text{TM} = \text{Cr}, \text{Mn}, \text{Cu}, \text{and Zn}$ ). The red curves are overlap populations for  $3d(\text{TM})-3p(\text{Ar})$ , green curves for  $4s(\text{TM})-3p(\text{Ar})$ , and black curves for  $4p(\text{TM})-3p(\text{Ar})$ . The *BDEs* of the complexes are 0.19, -0.25, 0.22, and -0.40 eV, respectively.

**Acknowledgements.** This work is supported by the Flemish Fund for Scientific Research (FWO-Vlaanderen), the KU Leuven Research Council (GOA 14/007) and the Deutsche Forschungsgemeinschaft within FOR 1282 (FI 893/4). VTN thanks the Vietnam National Foundation for Science and Technology Development (NAFOSTED) under grant 104.06-2013.06.

**Supplementary Information.** SI includes Tables and Figures providing more detailed information and is divided into four parts: analysis of the mass spectra, dependence of the cluster-*RG* binding energy on the used functionals, interaction of  $\text{Si}_n\text{Mn}^+$  ( $n = 6-10$ ) with rare gas atoms (Ar, Xe) and interaction of  $\text{Si}_7\text{TM}^+$  ( $\text{TM} = \text{Cr}, \text{Mn}, \text{Cu}$  and  $\text{Zn}$ ) with rare gas atoms (Ar, Xe).

## References

- [1] W. H. Robertson and M. A. Johnson, *Ann. Rev. Phys. Chem.*, 2003, **54**, 173-213.
- [2] W. Huang and L.-S. Wang, *Phys. Rev. Lett.*, 2009, **102**, 153401.
- [3] S. Gilb, K. Jacobsen, D. Schooss, F. Furche, R. Ahlrichs and M. M. Kappes, *J. Chem. Phys.*, 2004, **121**, 4619-4627.
- [4] A. Fielicke, C. Ratsch, G. von Helden and G. Meijer, *J. Chem. Phys.*, 2005, **122**, 091105.
- [5] C. Ratsch, A. Fielicke, A. Kirilyuk, J. Behler, G. von Helden, G. Meijer and M. Scheffler, *J. Chem. Phys.*, 2005, **122**, 124302.
- [6] a) A. Fielicke, C. Ratsch, G. von Helden and G. Meijer, *J. Chem. Phys.*, 2007, **127**, 234306; b) P. V. Nhat, V. T. Ngan and M. T. Nguyen, *J. Phys. Chem. C*, 2010, **114**, 13210-13218.
- [7] P. Gruene, A. Fielicke and G. Meijer, *J. Chem. Phys.*, 2007, **127**, 234307.
- [8] J. T. Lyon, P. Gruene, A. Fielicke, G. Meijer, E. Janssens, P. Claes and P. Lievens, *J. Am. Chem. Soc.*, 2009, **131**, 1115-1121.
- [9] V. T. Ngan, P. Gruene, P. Claes, E. Janssens, A. Fielicke, M. T. Nguyen and P. Lievens, *J. Am. Chem. Soc.*, 2010, **132**, 15589-15602.
- [10] R. Gehrke, P. Gruene, A. Fielicke, G. Meijer and K. Reuter, *J. Chem. Phys.*, 2009, **130**, 034306.
- [11] P. Gruene, D. M. Rayner, B. Redlich, A. F. G. van der Meer, J. T. Lyon, G. Meijer and A. Fielicke, *Science*, 2008, **321**, 674-676.
- [12] L. Lin, P. Claes, P. Gruene, G. Meijer, A. Fielicke, M. T. Nguyen and P. Lievens, *Chemphyschem*, 2010, **11**, 1932-1943.
- [13] a) K. R. Asmis, T. Wende, M. Brummer, O. Gause, G. Santambrogio, E. C. Stanca-Kaposta, J. Dobler, A. Niedziela and J. Sauer, *Phys. Chem. Chem. Phys.*, 2012, **14**, 9377-9388; b) C. Kerpál, D. J. Harding, A. C. Hermes, G. Meijer, S. R. Mackenzie and A. Fielicke, *The J. Phys. Chem. A*, 2012, **117**, 1233-1239.

- [14] J. L. F. Da Silva, C. Stampfl and M. Scheffler, *Phys. Rev. B*, 2005, **72**, 075424.
- [15] P. D. Carnegie, B. Bandyopadhyay and M. A. Duncan, *J. Phys. Chem. A*, 2011, **115**, 7602-7609.
- [16] J. E. Muller, *Appl. Phys. A: Mater. Sci. Process.*, 2007, **87**, 433-434.
- [17] P. D. Carnegie, B. Bandyopadhyay and M. A. Duncan, *J. Phys. Chem. A*, 2008, **112**, 6237-6243.
- [18] K. Hirsch, V. Zamudio-Bayer, F. Ameseder, A. Langenberg, J. Rittmann, M. Vogel, T. Möller, B. v. Issendorff and J. T. Lau, *Phys. Rev. A*, 2012, **85**, 062501.
- [19] W. Bouwen, P. Thoen, F. Vanhoutte, S. Bouckaert, F. Despa, H. Weidele, R. E. Silverans and P. Lievens, *Rev. Sci. Instrum.*, 2000, **71**, 54-58.
- [20] A. Fielicke, G. von Helden and G. Meijer, *Eur. Phys. J. D*, 2005, **34**, 83-88.
- [21] V. T. Ngan, E. Janssens, P. Claes, J. T. Lyon, A. Fielicke, M. T. Nguyen and P. Lievens, *Chem. Eur. J.*, 2012, **18**, 15788-15793.
- [22] Y. Zhao and D. Truhlar, *Theor. Chem. Acc.*, 2008, **120**, 215-241.
- [23] P. Pyykko, *J. Am. Chem. Soc.*, 1995, **117**, 2067-2070.
- [24] M. J. Frisch and et al. Gaussian 03, *Gaussian, Inc.: Wallingford, CT*, **2004**.
- [25] E. Janssens, P. Gruene, G. Meijer, L. Woste, P. Lievens and A. Fielicke, *Phys. Rev. Lett.*, 2007, **99**, 063401.
- [26] P. Claes, E. Janssens, V. T. Ngan, P. Gruene, J. T. Lyon, D. J. Harding, A. Fielicke, M. T. Nguyen and P. Lievens, *Phys. Rev. Lett.*, 2011, **107**, 173401.
- [27] V. Zamudio-Bayer, L. Leppert, K. Hirsch, A. Langenberg, J. Rittmann, M. Kossick, M. Vogel, R. Richter, A. Terasaki, T. Möller, B. v. Issendorff, S. Kümmel and J. T. Lau, *Phys. Rev. B*, 2013, **88**, 115425.
- [28] L. W. Bruch, M. W. Cole and E. Zaremba, *Clarendon, Oxford*, 1997, 229.
- [29] P. D. Carnegie, B. Bandyopadhyay and M. A. Duncan, *J. Chem. Phys.*, 2011, **134**, 014302.
- [30] P. Claes, Doctoral thesis, University of Leuven, 2012.
- [31] P. Ros and G. C. A. Schuit, *Theor. chim. acta*, 1966, **4**, 1-12.